Numerical Investigation of Cu_2O as Hole transport layer for High-Efficiency CIGS solar cell

Muhammad Hassan Yousuf, [1,] Faisal Saeed, [2,] * and Haider Ali Tauqeer[2]

1. Department of Electrical Engineering, University of Engineering and Technology (UET) Lahore, Lahore 54890, Punjab, Pakistan; 2020msee137@student.uet.edu.pk
2. Department of Electrical Engineering, SBASSE, Lahore University of Management Sciences (LUMS), Lahore 54792, Punjab, Pakistan; 19060005@lums.edu.pk, 190600036@lums.edu.pk

* Correspondence: 19060005@lums.edu.pk

Abstract: Copper indium gallium selenide (CIGS) is an inexpensive material that has the potential to dominate the next-generation photovoltaic (PV) industry. Here we detail computational investigation of CIGS solar cell with encouragement of adopting cuprous dioxide (Cu_2O) as a Hole Transport Layer (HTL) for efficient fabricated CIGS solar cells. Although Cu_2O as a HTL has been studied earlier for perovskite and other organic/inorganic solar cell yet no study has been detailed on potential application of Cu_2O for CIGS solar cells. With the proposed architecture, recombination losses are fairly reduced at the back contact and contribute to enhanced photo-current generation. With the introduction of Cu_2O, the overall cell efficiency is increased to 26.63%. The wide-band of Cu_2O pulls holes from the CIGS absorber which allows smoother extraction of holes with experiencing lesser resistance. Further, it was also inferred that, HTL also improves the quantum efficiency (QE) for photons with large wavelengths thus increases the cell operating spectrum.

Keywords: ***Cu_2O, CIGS, HTL, Buffer Layer, SCAPS***

1. Introduction

Thin-film copper indium gallium di-selenide [$Cu(In,Ga)Se_2$] or CIGSe technology is considered the most promising next-generation photovoltaic (PV) technology due to its direct bandgap (~1.0-1.14 eV), high absorption coefficient (~10^5 cm^{-1}), and lower material losses [1-6]. CIGS cells have the highest power conversion efficiency as compared to other thin-film technologies like Cu-chalcopyrite, cadmium telluride (CdTe), and amorphous silicon (a-Si), with a certified record efficiency of 23.40% for lab-scale cells[7]. CIGS material is inexpensive and can deposit on any rigid or flexible substrate which increases its applications in commercial and wearables devices as well [8-10]. CIGS solar cells exhibit outstanding stability, high efficiencies and radiation tolerance hence can also be used for space application [11].

CIGS is a direct bandgap p-type semiconductor that minimizes the requirement of large diffusion length and also decreases losses. Such semiconductor with high absorption co-efficient is ideal for thin-film PV technology [12]. The tunable bandgap of p-type $CuIn_{1-x}Ga_xSe_2$ can be adjusted by varying the concentration of gallium and indium, to match the solar spectrum[13]. A thicker CIGS layer means more material which results in higher cost, particularly indium which is a costly material and its availability will be an issue in the future [14]. Aluminum (Al)/Nickle (Ni) and molybdenum (Mo) act as front and rear contact for the cell while Magnesium fluoride (MgF_2) acts as an anti-reflecting coating. Mo deposited on substrates offers lower electrical resistance (< 0.5 Ω/sq.), higher thermal stability, and also less resistance to p-CIGSe by forming a thin layer of molybdenum di-selenide ($MoSe_2$) during the absorber formation [15].

The optimum band gap for CIGS is ~1.14 eV due to material properties[16, 17]. In general, for efficient absorption, a bandgap of ~1.4eV is required to match the solar spectrum. In CIGS crystal Indium can replaced by Gallium to achieve the required optical bandgap, hence by the introduction of Indium the bandgap of CIGS can be varied from 1.04 eV to 1.7 eV. Other elements can also be used in chalcopyrite $Cu(In,Ga,Al)(S,Se)_2$, this can vary bandgap from 1.04 eV ($CuInSe_2$) to about 3.5 eV ($CuAlS_2$) covering most of the visible spectrum. However, for CIGS material a higher bandgap causes complications. The efficiency of the cell decreases because of defect states and dangling bonds. For a wider bandgap, the defect level is in the middle of the bandgap thus increasing the bandgap also increases defect levels[18]. Fig. 1 [19] depicts a scanning electron microscope image (SEM) of a CIGS cell. In this substrate configuration, the light enters through a transparent conductive oxide (TCO) i.e., zinc oxide (ZnO) layer. The working of CIGS cell is as follows: n-type cadmium sulfide (CdS) buffer layer (bandgap, E_g~2.4 eV) absorbs the higher energy photons $\geq 2.4\ eV$, while photons of energy less than $2.4\ eV$ are transmitted to the p-type CIGS absorber layer where electron-hole pairs are mainly generated. Due to in-built junction voltage of n-CdS/p-CIGS, the electrons within the diffusion length are carried away from the p-CIGS layer to the n-CdS layer and are collected at the n-type electrode. Similarly, holes are carried away from the n-type buffer layer to the p-type absorber layer and are collected at the p-type electrode. A highly transparent, large bandgap (>3.3 eV) n-type TCO layer i.e., ZnO act as front contact over CdS called window layer. Typically, ZnO (E_g~3.2 eV) the layer consists of a double layer of a thick (400nm) layer of n-doped ZnO layer and a thin (50nm) intrinsic ZnO. The intrinsic-zinc oxide (i-ZnO) provides isolation between CdS and n-doped ZnO (ZnO: Al) so that i-ZnO prevents the diffusion of Al into the CdS/CIGS absorber layer.

Preprints (www.preprints.org) | NOT PEER-REVIEWED | Posted: 22 October 2021 doi:10.20944/preprints202110.0326.v1

The buffer layer acts as an intermediate layer between the window layer and absorber layer which provides stability [20, 21] . The buffer layer is highly-resistive and it prevents shunting between the absorber layer and TCO i.e., ZnO. The buffer layer affects the band offset and electric field in the junction, and thus improves the charge transport [22]. CdS is the most common material used as a buffer layer. The narrow bandgap of CdS causes current losses due to parasitic absorption. Additionally, cadmium (Cd) is a toxic element and is classified as a human carcinogen. For these reasons, extensive research is being done on the alternative buffer layer, such as Zinc sulfides, oxides, and selenides[23-26]. Like CdS, zinc selenide (ZnSe) is an n-type semiconductor but with a wide bandgap and the most promising material to replace CdS [27-30]. The bandgap of ZnSe is $E_g \sim 2.9\ eV$ which is greater than the CdS $E_g \sim 2.4\ eV$, that means more light is passed to the CIGS absorber layer and the larger number of photocarriers will be generated increasing efficiency.

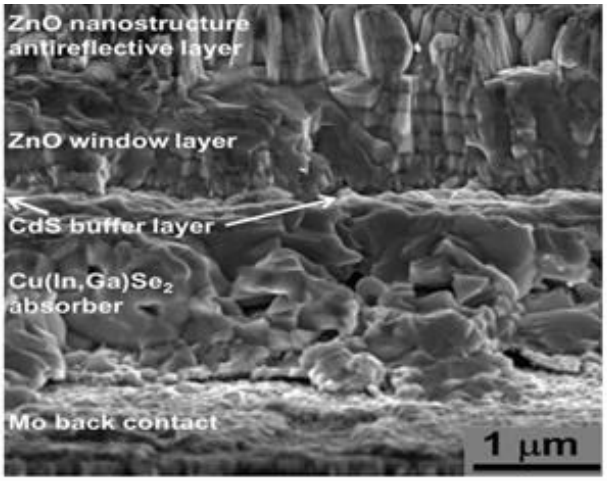

Fig.1. Scanning Electron Image (SEM) of buffer layered CIGS solar cell [19]

This research effort proposes a theoretical approach to enhance the power conversion efficiency (PCE) of the CIGS solar cells with structure Mo/Cu_2O/CIGS/buffer layer/intrinsic-i-ZnO/n-doped ZnO. The CIGS modeling and analyses are done by using a solar cell capacitance simulator (SCAPS-1D) that gives simulation results close to fabrication results[21, 31-35]. Here CdS is re-placed with is replaced by a double buffer layer CdS/ZnSe. In addition to the double buffer layer, the Cu_2O is implemented as the hole transport layer (HTL). Cu_2O is an earth-abundant, non-toxic material and is easy to fabricate. The thickness of the CIGS absorber layer is reduced to 850nm which is usually about 3000nm. Under standard illumination (AM1.5 G, 100 mW/cm^2, 300 K) [36], the photovoltaic parameters, short circuit current density (J_{sc}), open-circuit voltage (V_{oc}), fill factor (FF), and efficiency (η) of different hole transport layers and buffer layers under varied thicknesses are measured.

Cu_2O is a p-type semiconductor and has an optical bandgap of 2.17 eV. Its application as photovoltaic material lies in the fact that the constituent materials are nontoxic and abundantly available on the earth, and that the Cu_2O has a high absorption coefficient in visible regions and low-cost producibility. Doping concentration in Cu_2O can be achieve up to 10^{17} cm^3 [37].

Cuprite Cu_2O is known to have a low value of thermal expansion coefficient around room temperature, and to exhibit a negative thermal-expansion behavior at low temperatures. The thermal decomposition temperature of Cu_2O exceeds 900 ^{O}C. So, for the high temperature processing of CIGS material, may not have any serious effect of the Cu_2O layer [38]. Moreover, there is possibility of Cu diffusion in CIGS material at the rear end which can change the CIGS bandgap and its performance. This can be address by the grading process of CIGS structure and the exact bandgap of CIGS can be achieved from In/Ga ratio to compensate for Cu diffusion.

As compared to conventional CIGS cells the device with Cu_2O as HTL gives greater output voltage. To optimize the light absorption and output current we put forward Cu_2O as HTL for further enhancement.

2. Novelty

Theoretical studies show the significant increase in the efficiency of chalcopyrite based solar cells with the introduction of Ga_2O_3, MoO_3, $MoSe_2$ and MoS_2 as back interface. MoO_3 gives maximum efficiency of 24% among all due to its highest bandgap [39-41]. Bandgap of Cu_2O make it suitable to work as back interface for CIGS solar cells. Although for perovskite and copper zinc tin sulfide (CZTS) extensive studies are present on Cu_2O as HTL but for CIGS, it's a novel approach. Here different parameters of CIGS cells are observed using SCAPS. It is observed by numerical calculations that Cu_2O increases the flow of charge carriers which greatly enhances the efficiency of CIGS cells. As compared to conventional CIGS cells the device with Cu_2O as HTL gives greater output voltage. By using Cu_2O recombination losses were reduced which results in high efficiency and stability. As Cu_2O is a transparent and inexpensive inorganic material it does not increase the cost and complexity of cell fabrication.

Preprints (www.preprints.org) | NOT PEER-REVIEWED | Posted: 22 October 2021 doi:10.20944/preprints202110.0326.v1

3. Materials and Methods

3.1. Numerical Modeling

Fig. 2 depicts the proposed CIGS solar cell with a p-type CIGS absorber layer and a thin layer of Mo deposited on a glass substrate. An n-type ZnSe material acts as a buffer layer and n-ZnO acts as a window layer. The proposed structure is simulated on SCAPS-1D software which solves semiconductor equations, the equation of continuity, and the Poisson equation for electrons and holes. These equations are as follows [42]:

$$\frac{d^2}{dx^2}\psi(x) = \frac{e}{\varepsilon_0 \varepsilon_r} \left[p(x) - n(x) - N_a + N_d + p_t(x) - n_t(x) \right] \quad (1)$$

Where ψ is electrostatic potential, e is electric charge, $\varepsilon_0, \varepsilon_r$ is the electric permittivity of vacuum and relative electric permittivity, $p(x)$ and $n(x)$ are the concentration of free holes and electrons, N_a, N_d are ionized acceptor and donor concentration, $p_t(x), n_t(x)$ are the concentration of trapped holes and electrons.

$$\frac{\partial \Delta p}{\partial t} = G_P - \frac{\Delta p}{\tau_p} + D_p \frac{\partial^2 \Delta p}{\partial x^2} + \mu_P \frac{\partial E}{\partial x} \Delta p + \mu_P E \frac{\partial \Delta p}{\partial x} \quad (2)$$

$$\frac{\partial \Delta n}{\partial t} = G_n - \frac{\Delta n}{\tau_n} + D_n \frac{\partial^2 \Delta n}{\partial x^2} + \mu_n \frac{\partial E}{\partial x} \Delta n + \mu_n E \frac{\partial \Delta n}{\partial x} \quad (3)$$

Where $\Delta p, \Delta n$ is change in holes and electron concentration, G is generation rate of holes and electrons, τ_p , τ_n is hole and electron lifetime, D is diffusion coefficient, μ_n , μ_P is the mobility of holes and electrons and E is the electric field. SCAPS numerically calculate a steady-state solution of these equations with appropriate boundary conditions [43].

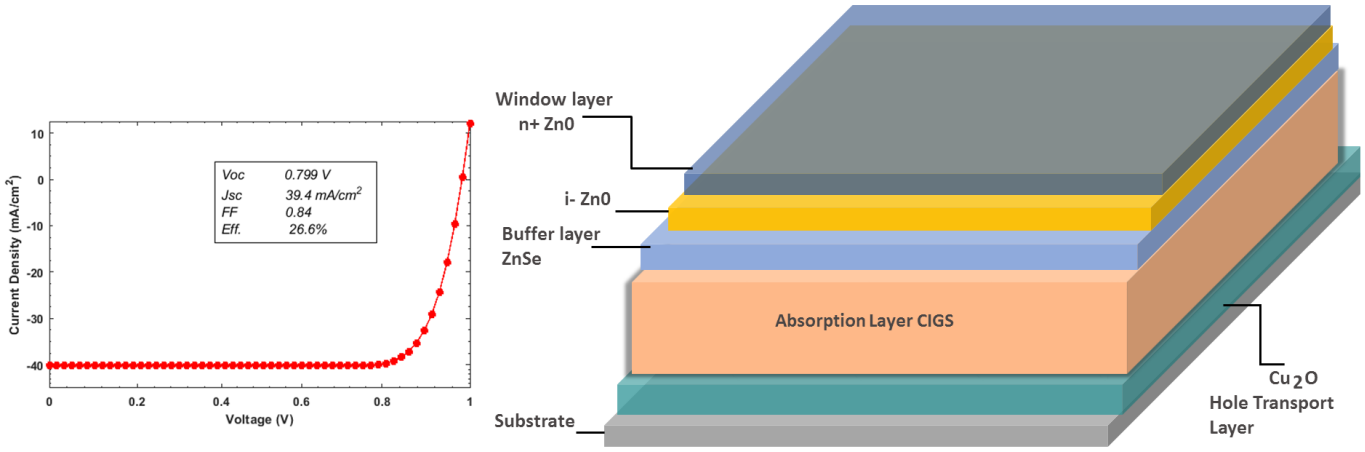

Fig. 2. (a) J-V curve of simulated cell (b)Proposed CIGS solar cell architecture

3.2. Material Parameters

The basic parameters used for simulation for the proposed CIGS solar cell are shown in the Table 1. The thickness of the CIGS layer is 850 nm while the thickness of each buffer layer is varied from 20 nm to 100 nm at a time to observe the behavior and optimize thickness for maximum efficiency.

Preprints (www.preprints.org) | NOT PEER-REVIEWED | Posted: 22 October 2021 doi:10.20944/preprints202110.0326.v1

TABLE 1. Material Parameters for SCAPS

Parameters	Cu_2O [44]	CIGS [45]	ZnSe [45]	i-ZnO [45]	n+ZnO [45]
Thickness (nm)	20	850	50	50	400
Energy Bandgap, E_g (eV)	2.17	1.16	2.9	3.3	3.2
Electron affinity, χ (eV)	3.2	4.0	4.2	4.4	4.4
Relative Permittivity, ε_r	7.1	13.6	10	9	9
Density of states at Conduction Band, N_c (cm^{-3})	2×10^{17}	2.0×10^{17}	1.0×10^{18}	3.1×10^{18}	3.1×10^{18}
Density of states Valance Band, N_v (cm^{-3})	1.1×10^{19}	1.5×10^{19}	1.8×10^{19}	1.8×10^{19}	1.7×10^{19}
Electron Mobility, μ_e (cm^2/Vs)	200	100	70	100	100
Hole Mobility, μ_h (cm^2/Vs)	80	25	3	31	31
Acceptor Concentration, N_a (cm^{-3})	1.0×10^{18}	1.0×10^{16}	0	0	0
Donor Concentration, N_d (cm^{-3})	0	0	5.5×10^{17}	1.0×10^{18}	1.0×10^{19}
Defect Density, N_t (cm^{-3})	1.0×10^{14}	1.0×10^{15}	1.0×10^{18}	1.0×10^{14}	1.0×10^{14}

4. Results

4.1. Effect of ZnSe layer thickness

As illustrated in Fig.3, the thickness of ZnSe was varied from 20nm to 100nm and its effect on basic photovoltaic parameters η, FF, V_{oc}, J_{sc} was observed. With the increase in the thickness of ZnSe, the output voltage V_{oc} decreases gradually from 0.85003 to 0.84994 V, a decrease of 0.10% is observed while current density J_{sc} changes from 37.05 to 36.7 mA/cm^2. From efficiency η formula (4) and fill factor (5), efficiency decreases from 26.71 to 26.62% an overall decrease of about 1%, and FF increases from 84.84 to 85.35% an increase by .51%,

As the thickness of the ZnSe layer increases the efficiency decreases which can be attributed to the carrier recombination. As thickness increases the recombination rate within the CIGS absorber layer due to the increase of conduction band edge which opposes the charge separation. This has little effect on overall device performance because it has a larger bandgap while a lesser number of carriers have little effect on the depletion region.

$$\eta = \frac{J_{max}\ V_{max}}{A_t P_{in}} \tag{4}$$

$$FF = \frac{J_{max}\ V_{max}}{J_{sc}\ V_{oc}} \tag{5}$$

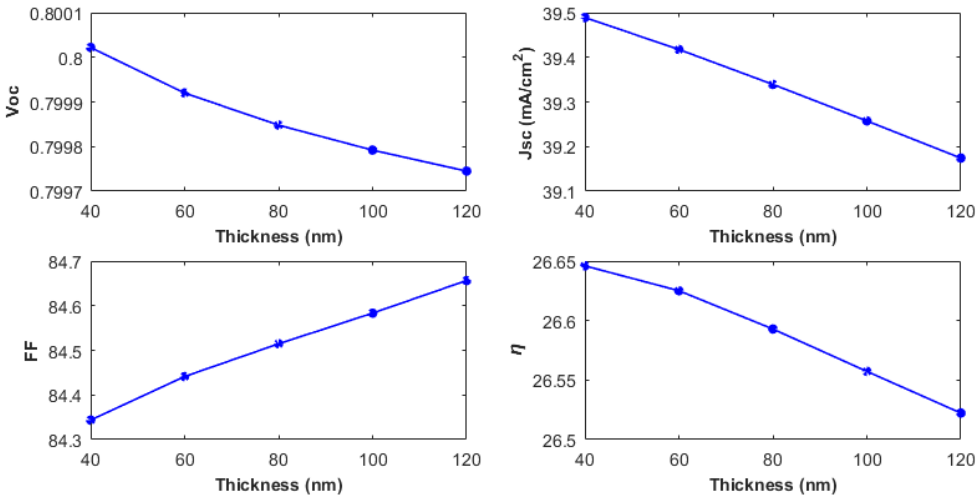

Fig.3. Impact of varying ZnSe layer thickness on open circuit voltage, short circuit density, fill factor and efficiency of the solar cell under standard global solar spectrum

Preprints (www.preprints.org) | NOT PEER-REVIEWED | Posted: 22 October 2021 doi:10.20944/preprints202110.0326.v1

4.3. External Quantum Efficiency

Fig.5 depicts the response of proposed absorption of incident photons and is represented as a quantum efficiency (QE) graph. Here with the lower thickness of the CdS layer, QE is higher as compared to higher thickness at the same wavelength. Fig. 6 shows QE at different ZnSe thickness, which shows a similar response but here at a lower wavelength, the thickness of ZnSe has very little effect in QE.

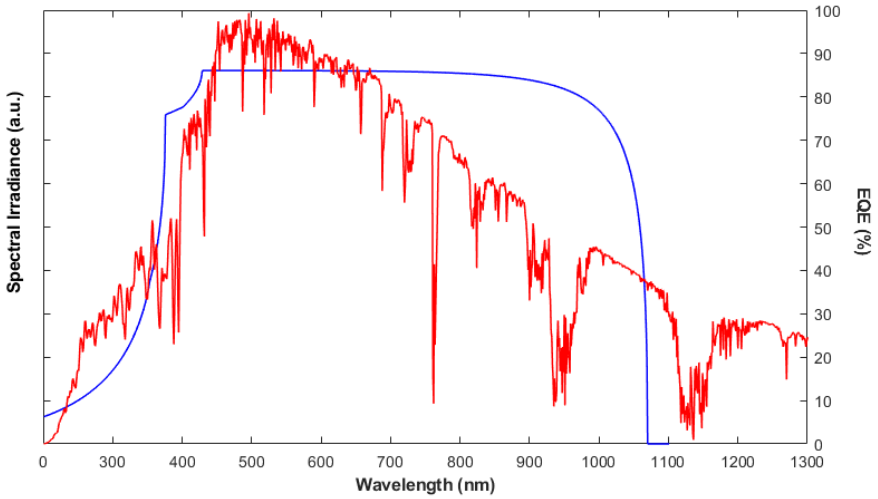

Fig.5. Effect of ZnSe buffer layer on Quantum Efficiency of the solar cell

4.4. Effect of Hole Transport Layer (HTL)

Fig.11. shows an increase in the efficiency of CIGS cells with the introduction of a thin layer of Cu_2O as an HTL. Cu_2O decreases the recombination of photo-generated carriers at the CIGS absorber layer thus increase the number of carriers that contribute to photo-current [46, 47]. The wide-band of Cu_2O reduces recombination losses and pulls holes from the CIGS absorber. This allows smoother extraction of holes with experiencing lower resistance. The proposed CIGS cell with HTL shows an increase in output, Voc, and Jsc as compared to cell without HTL and η increases from 21.04 to 26.63%, a total increase of 6.12% is recorded. This increase in efficiency can also be attributed to the p-type semiconductor nature of Cu_2O. The high absorption coefficient of Cu_2O allows to absorb photons and contribute in photocurrent as recombination in this region is minimum. The absorption in Cu_2O can also be observed if the cell is simulated in inverted manner.

4.5 Optical Losses

For CIGS, the absorption coefficient, α in the photon energy range $h\nu < E_g$ is $\alpha = 4\pi k/\lambda$= (4-5) ×10^3 cm^{-1} [48]. For these values of α should result in a high value of quantum efficiency but this is not observed in this case. For $\lambda > \lambda_g = hc / E_g$ the quantum efficiency decreases drastically to zero within a range of 100 nm above λ_g. This rapid decrease of quantum efficiency can be attributed to the 'band tails' of the density of states which is due to disordered crystal structures and strong doping in the semiconductor. The force field of impurity atom and wave function of electrons overlap and transformed into an impurity band. At critical concentration, the conduction band joins with the impurity band which results in tails of the density of states. The absorption coefficient depends exponentially on incident photon energy.

$$\alpha = \alpha_0 \, exp\left[\frac{h\nu - E_0}{E_U \; T}\right] \qquad (6)$$

Where E_U is Urbach energy, these empirical dependencies are represented by the Urbach rule [49]. For an electron to take part in photogenerated current it must absorb energy greater than or equal to E_g. In the case of tail absorption at $h\nu < E_g$, the

Preprints (www.preprints.org) | NOT PEER-REVIEWED | Posted: 22 October 2021 doi:10.20944/preprints202110.0326.v1

electron gets energy equal to $h\nu$ from the incident photon and the rest is covered by phonons. The Urbach rule represents that as $h\nu$ decreases, the probability of the multiphonon process also decreases. The electron absorbed a photon having energy $h\nu < E_g$ takes part in photocurrent just as that of $h\nu \geq E_g$. The part of spectrum $h\nu < E_g$ makes a small contribution to short circuit current 0.40 mA/cm^2 (1.10%). For spectral range $h\nu \geq E_g$ absorption coefficient follows direct-bandgap law for semiconductors.

$$\alpha = \alpha_0 \frac{\sqrt{h\nu - E_g}}{h\nu} \tag{7}$$

For CIGS material with a bandgap $E_g = 1.16$ eV the wavelength is given by, $\lambda_g = hc/E_g$ =1068 nm and can be observed from Fig.7

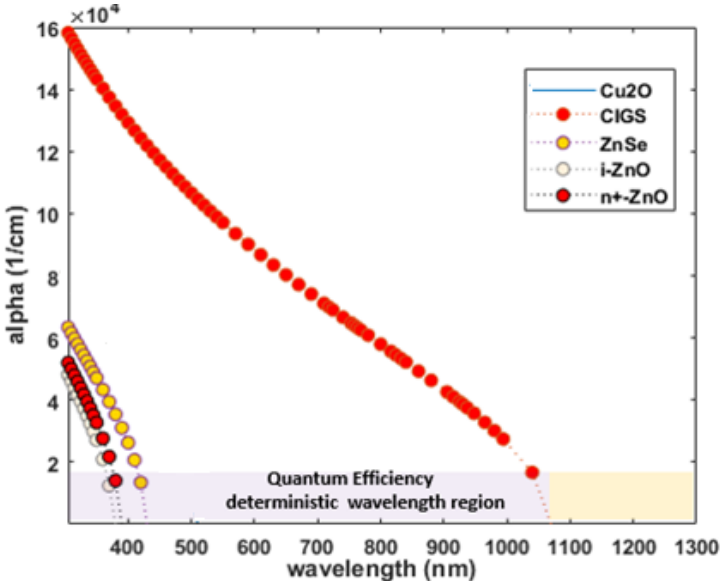

Fig.7. Layers optical absorption constant behavior as a function of wavelength across the solar spectrum

4.6. Absorption and Reflective losses

Optical losses can be calculated quantitively by calculating short circuit current density J_{sc}. If $h\nu$ is the photon energy and ϕ_i is the spectral radiation power density, J_{sc} can be written as follows.

$$J_{sc} = q \sum_i \frac{\phi_i \lambda_i}{h\nu} T(\lambda_i)\ \eta\ \Delta\lambda_i \tag{8}$$

Where q is the charge on the electron, η is the quantum efficiency here assumes $\eta = 1$, $T(\lambda_i)$ is the transmission of photons from one layer to the other, the summation in the above equation should range from $\lambda = 300\ nm$ to $\lambda_g = hc/E_g = 1068\ nm$ for bandgap $E_g = 1.16$ eV. For such CIGS cells, the total reflection losses are about 8.1% and total absorption losses are 9.4% which adds up to 17.5% of total optical losses.

4.7. Recombination Losses

Charges created from the absorption of incident photons in the space charge region (SCR) move due to the electric field across the junction, electrons towards the front ZnO layer, and holes towards the neutral CIGS layer to further Cu_2O and back contact of Mo contact. However not all photogenerated charges contribute to the photocurrent, some of these carriers recombine inside the SCR before reaching the electrodes. Recombination can also occur at front surface, outside space charge region, and back surface CIGS/metal interface. Recombination mainly occurs at the interfaces of ZnSe/CIGS is due to discontinuity in the conduction band. The spikes in the recombination curve at interfaces can be observed in Fig.8.

The lifetime of minority carrier determines the diffusion length, $L = \sqrt{\tau D}$ and has an impact on efficiency [50]. Recombination losses mainly depend upon carrier lifetime and width of SCR which is calculated from the concentration of uncompensated acceptors $N_a - N_d$. For a CIGS absorber layer, the width of SCR is determined from following relation [51].

Preprints (www.preprints.org) | NOT PEER-REVIEWED | Posted: 22 October 2021 doi:10.20944/preprints202110.0326.v1

$$W_{SCR} = \frac{1}{q}\sqrt{\frac{2\varepsilon_0\varepsilon\ (\phi_{bi}-qV)}{N_a-N_d}} \quad (9)$$

Where ϕ_{bi} is barrier height, equals $\phi_{bi} = qV_{bi}$, and V_{bi} is the diffusion potential, for CIGS relative permittivity equals ($\varepsilon = 13.60$) and $N_a - N_d$ is uncompensated acceptor concentration.

From Fig 8, at higher $N_a - N_d$ width of SCR will decrease and with the decrease in absorption area the cell's efficiency decreases. With the decrease in $N_a - N_d$, the width of SCR increases which gives higher quantum efficiency as more incident photons are absorbed in wider SCR and photocarriers reach the boundaries without recombination. However, expansion in SCR from above some extant reduces the electric field inside SCR which in result cause recombination at the surface.

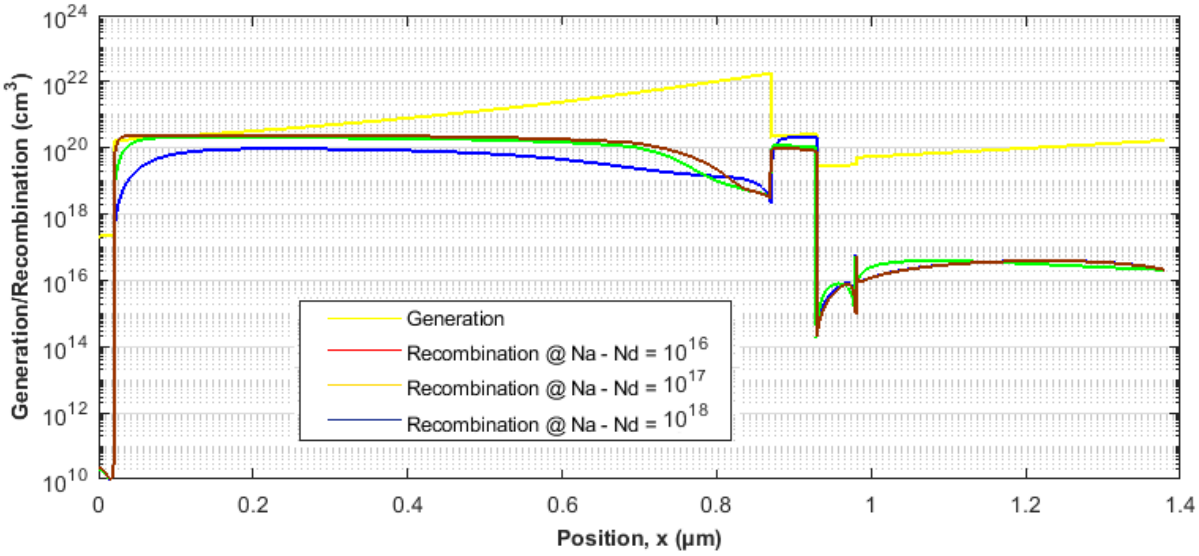

Fig.8. Generation/Recombination profile

4.8. Recombination Losses inside SCR

Recombination of carriers inside SCR can be calculated by using the Hecht equation [52].

$$\eta\ (x) = \frac{\lambda_p}{W_{SCR}}\left[1 - exp\left(-\frac{x}{\lambda_p}\right)\right] + \frac{\lambda_n}{W_{SCR}}\left[1 - exp\left(-\frac{W_{SCR}-x}{\lambda_n}\right)\right] \quad (10)$$

Where λ_n and λ_p are drift length of electrons and holes inside SCR, x is coordinate at which electron-hole pair is generated measured from ZnSe/CIGS interface. If electric field strength is E, mobility is μ and carrier lifetime is τ, the drift lengths for electron-holes in SCR can be expressed by the following relations.

$$\lambda_n = \mu_n\tau_n E \quad (11)$$

$$\lambda_p = \mu_p\tau_p E \quad (12)$$

From the above equation, the charge collection efficiency for an interval equals to $\eta(x)\alpha_i e^{-\alpha x}$, hence the quantum efficiency for an incident photon with a wavelength λ_i is calculated by the following expression

$$\eta(\lambda_i) = \int_0^W \eta(x)\alpha_i e^{-\alpha x}\ dx \quad (13)$$

Preprints (www.preprints.org) | NOT PEER-REVIEWED | Posted: 22 October 2021 doi:10.20944/preprints202110.0326.v1

4.9. Energy Band Diagram

In Fig.9 the energy band diagram of the CIGS cell shows the band alignment of buffer layer ZnSe and Cu_2O hole transport layer. The buffer layer is efficient due to the band alignment of the CIGS/ZnSe interface. The Cu_2O reduces recombination losses and attracts photogenerated holes inside CIGS absorber. This allows smoother extraction of holes with experiencing lower resistance.

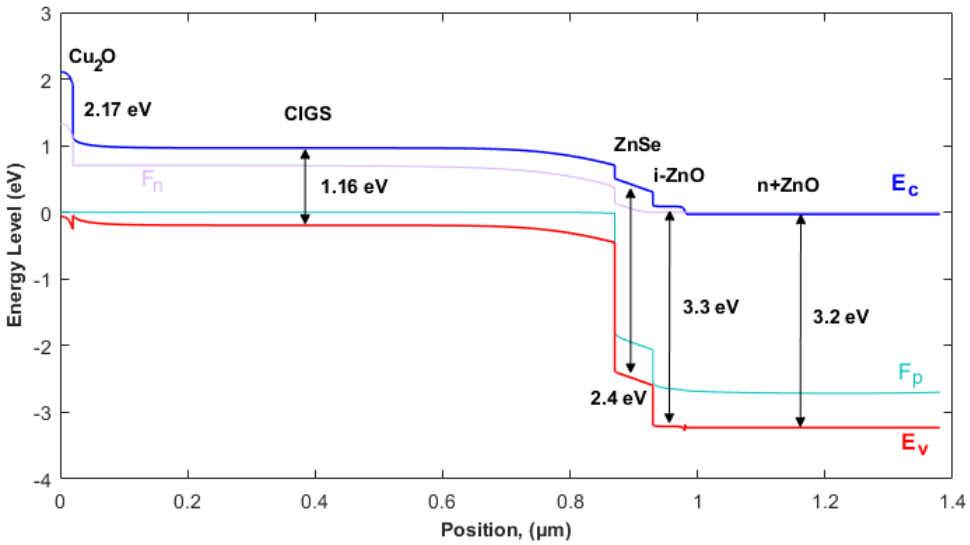

Fig.9. Energy band diagram of the proposed CIGS solar cell

4.10. Results Comparison

Table 2 and Fig. (10&11) illustrate a comparison of basic photovoltaic parameters among conventional buffer layer of CdS, ZnSe, and ZnSe along with Cu_2O as hole transport layer. The PCE of CIGS cells with HTL is much larger than conventional CIGS cells. As compared to the solar cells with only CdS as buffer layer 20.77% and with ZnSe as double buffer layer it increases to 21.04%. with the introduction of Cu_2O as HTL, the overall efficiency increases up to 26.63%.

TABLE 2. Summary of Impact of Buffer layer and Hole Transport Layer

Materials	**CdS**	**ZnSe**	**ZnSe/Cu_2O**
Voc (V)	0.7599	0.7599	0.8543
Jsc(mA/cm^2)	35.04	34.92	37.09
FF (%)	77.99	79.27	86
η (%)	20.77	21.04	26.63

Preprints (www.preprints.org) | NOT PEER-REVIEWED | Posted: 22 October 2021 doi:10.20944/preprints202110.0326.v1

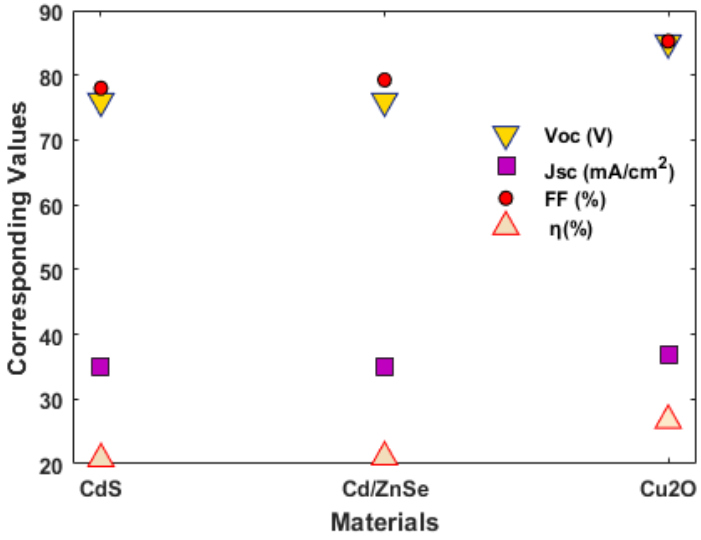

Fig.10. Comparative illustration of electrical parameters of proposed CISG solar cell; open circuit voltage, short circuit current density, fill factor and efficiency by the selection of optimal layer thickness of a single buffer layer CdS, double buffer layer CdS/ZnSe and Cu_2O a hole transport layer. In the Figure, open circuit voltage is shown after multiplication of Voc with 100 i.e., 100 x Voc to clearly indicate the comparison of results.

5. Conclusions

In this study, CIGS cell with Cu_2O as the hole transport layer and ZnSe as buffer layers is investigated. CIGS cells give about 20% efficiency with CdS as the buffer layer. With the introduction of the hole transport layer photovoltaic parameters, Voc and Jsc increase further and overall efficiency increases up to 26.63%. Here Cu_2O has a key role in the transmission of photo-carriers and reduces the carrier recombination which enhances the overall performance of the solar cell. The wide-band of Cu_2O pulls holes from the CIGS absorber. This allows smoother extraction of holes with experiencing lower resistance. The results presented here give parameters for the fabrication of high-efficiency CIGS solar cells.

The results presented here are obtained from the theoretical calculation which represents the effectiveness of HTL which enhances the efficiency by reducing recombination losses in the absorber layer. CIGS solar cells have lower lab-scale efficiency of about 25% than Si-cells. The numerical calculations represent the increase in efficiency by the addition of HTL. Based on this study it is suggested that CIGS cells with HTL can be a major part of the Solar industry due to higher efficiency and stability.

Funding: This research received no external funding.

Acknowledgments: The author acknowledges Dr. Marc Burgelman, University of Gent, for providing the SCAPS-1D software for simulation of CIGS solar cell.

Conflicts of Interest: The authors declare no conflict of interest

References

1. F. Ahmad, T. H. Anderson, P. B. Monk, and A. J. A. o. Lakhtakia, "Efficiency enhancement of ultrathin CIGS solar cells by optimal bandgap grading," **58**, 6067-6078 (2019).
2. Y.-J. J. O. e. Chang, "Suppressing lossy-film-induced angular mismatches between reflectance and transmittance extrema: optimum optical designs of interlayers and AR coating for maximum transmittance into active layers of CIGS solar cells: erratum," **23**, A947-A948 (2015).

3. I. Massiot, A. Cattoni, and S. J. N. E. Collin, "Progress and prospects for ultrathin solar cells," **5**, 959-972 (2020).
4. Saeed, F.. W.M.D.. R.T.U.. K.M.A.. K.M.H. and G.H.. A Comparative Study of Grid-Tied PV Systems Employing CIGS and Crystalline Solar Modules. In Proceedings of the 2021 Mohammad Ali Jinnah University International Conference on Computing (MAJICC); IEEE, 2021; pp. 1–7.
5. S. Shi, L. Yao, P. Ma, Y. Jiao, X. Zheng, D. Ning, M. Chen, F. Sui, H. Liu, and C. J. M. T. E. Yang, "Recent progress in high temperature resistance PI substrate with low CTE for CIGS thin film solar cells," 100640 (2021).
6. Saeed, F.; Tauqeer, H.A.; Idrees, A.; Ali, M.Z.; Raza, A.; Khan, M.A. Buffer Layered PbS Colloidal Quantum Dot Solar Cell with Enhanced Efficiency. In Proceedings of the 2021 4th International Conference on Energy Conservation and Efficiency, ICECE 2021 - Proceedings; 2021.
7. D. Aiken, E. Dons, S.-S. Je, N. Miller, F. Newman, P. Patel, and J. J. I. J. o. P. Spann, "Lattice-matched solar cells with 40% average efficiency in pilot production and a roadmap to 50%," **3**, 542-547 (2012).
8. S. Cao, D. Yu, Y. Lin, C. Zhang, L. Lu, M. Yin, X. Zhu, X. Chen, D. J. A. a. m. Li, and interfaces, "Light Propagation in Flexible Thin-Film Amorphous Silicon Solar Cells with Nanotextured Metal Back Reflectors," **12**, 26184-26192 (2020).
9. A. Chirilă, P. Reinhard, F. Pianezzi, P. Bloesch, A. R. Uhl, C. Fella, L. Kranz, D. Keller, C. Gretener, and H. J. N. m. Hagendorfer, "Potassium-induced surface modification of Cu (In, Ga) Se 2 thin films for high-efficiency solar cells," **12**, 1107-1111 (2013).
10. K.-J. Yang, S. Kim, S.-Y. Kim, K. Ahn, D.-H. Son, S.-H. Kim, S.-J. Lee, Y.-I. Kim, S.-N. Park, and S.-J. J. N. c. Sung, "Flexible Cu 2 ZnSn (S, Se) 4 solar cells with over 10% efficiency and methods of enlarging the cell area," **10**, 1-10 (2019).
11. P. Reinhard, F. Pianezzi, B. Bissig, A. Chirilă, P. Blösch, S. Nishiwaki, S. Buecheler, and A. N. J. I. J. o. P. Tiwari, "Cu (In, Ga) Se $ _ {\bf 2} $ Thin-Film Solar Cells and Modules—A Boost in Efficiency Due to Potassium," **5**, 656-663 (2014).
12. A. Bouloufa, K. Djessas, and A. J. T. S. F. Zegadi, "Numerical simulation of CuIn {sub x} Ga {sub 1-x} Se {sub 2} solar cells by AMPS-1D," **515**(2007).
13. M. Latha, R. A. Devi, and S. J. O. M. Velumani, "Hot injection synthesis of Cu (In, Ga) Se2 nanocrystals with tunable bandgap," **79**, 450-456 (2018).
14. K. Ramanathan, R. Noufi, B. To, D. Young, R. Bhattacharya, M. Contreras, R. Dhere, and G. Teeter, "Processing and properties of sub-micron CIGS solar cells," in *2006 IEEE 4th World Conference on Photovoltaic Energy Conference*, (IEEE, 2006), 380-383.
15. S. R. Kodigala, "Cu (In1− xGax) Se2 and CuIn (Se1− xSx) 2 Thin Film Solar Cells," in *Thin films and nanostructures* (Elsevier, 2010), pp. 505-679.
16. S. Gharibzadeh, I. M. Hossain, P. Fassl, B. A. Nejand, T. Abzieher, M. Schultes, E. Ahlswede, P. Jackson, M. Powalla, and S. J. A. F. M. Schäfer, "2D/3D Heterostructure for Semitransparent Perovskite Solar Cells with Engineered Bandgap Enables Efficiencies Exceeding 25% in Four-Terminal Tandems with Silicon and CIGS," **30**, 1909919 (2020).
17. Y. Kamikawa, J. Nishinaga, H. Shibata, S. J. A. A. M. Ishizuka, and Interfaces, "Efficient Narrow Band Gap Cu (In, Ga) Se2 Solar Cells with Flat Surface," **12**, 45485-45492 (2020).
18. J. Ramanujam, U. P. J. E. Singh, and E. Science, "Copper indium gallium selenide based solar cells–a review," **10**, 1306-1319 (2017).
19. Y. J. N. S. C. Tang, "Copper indium gallium selenide thin film solar cells," 183-200 (2017).
20. Q. Du, B. Li, S. Shi, K. Zhang, Y. Zhang, S. Cheng, Z. Zhou, F. Liu, S. Sun, and Y. J. C. Sun, "Relationship between the intermediate phases of the sputtered Zn (O, S) buffer layer and the conduction band offset in Cd-free Cu (In, Ga) Se 2 solar cells," **22**, 4416-4426 (2020).
21. L. Wang, D.-B. Li, K. Li, C. Chen, H.-X. Deng, L. Gao, Y. Zhao, F. Jiang, L. Li, and F. J. N. E. Huang, "Stable 6%-efficient Sb 2 Se 3 solar cells with a ZnO buffer layer," **2**, 1-9 (2017).
22. A. O. Pudov, "Impact of secondary barriers on copper-indium-gallium-selenide solar-cell operation," (Colorado State University, 2005).
23. T. Feurer, P. Reinhard, E. Avancini, B. Bissig, J. Löckinger, P. Fuchs, R. Carron, T. P. Weiss, J. Perrenoud, S. J. P. i. P. R. Stutterheim, and Applications, "Progress in thin film CIGS photovoltaics–Research and development, manufacturing, and applications," **25**, 645-667 (2017).

24. C. Huang, S. S. Li, W. Shafarman, C.-H. Chang, E. Lambers, L. Rieth, J. Johnson, S. Kim, B. Stanbery, T. J. S. e. m. Anderson, and s. cells, "Study of Cd-free buffer layers using Inx (OH, S) y on CIGS solar cells," **69**, 131-137 (2001).
25. X. Y. Kong, D. Yu, Z. Huang, W. Shen, and N. Dai, "Atomic layer deposition for photovoltaics: applications and prospects," in *Optical Nanostructures and Advanced Materials for Photovoltaics*, (Optical Society of America, 2015), PTu3B. 1.
26. N. Mufti, T. Amrillah, A. Taufiq, M. Diantoro, and H. J. S. E. Nur, "Review of CIGS-based solar cells manufacturing by structural engineering," **207**, 1146-1157 (2020).
27. A. Ashok, G. Regmi, A. Romero-Núñez, M. Solis-López, S. Velumani, and H. J. J. o. M. S. M. i. E. Castaneda, "Comparative studies of CdS thin films by chemical bath deposition techniques as a buffer layer for solar cell applications," 1-20 (2020).
28. F. Ghamsari-Yazdel, I. Gharibshahian, and S. J. J. o. M. S. M. i. E. Sharbati, "Thin oxide buffer layers for avoiding leaks in CIGS solar cells; a theoretical analysis," 1-11 (2021).
29. R. Sharma, S. Patel, S. Chander, M. Kannan, and M. J. P. L. A. Dhaka, "Physical properties of ZnSe thin films: Air and vacuum annealing evolution to buffer layer applications," **384**, 126097 (2020).
30. F. Takagi, Y. Kageshima, K. Teshima, K. Domen, H. J. S. E. Nishikiori, and Fuels, "Enhanced photoelectrochemical performance from particulate ZnSe: Cu (In, Ga) Se 2 photocathodes during solar hydrogen production via particle size control," **5**, 412-423 (2021).
31. I. M. De Los Santos, H. J. Cortina-Marrero, M. Ruíz-Sánchez, L. Hechavarría-Difur, F. Sánchez-Rodríguez, M. Courel, and H. J. S. E. Hu, "Optimization of CH3NH3PbI3 perovskite solar cells: A theoretical and experimental study," **199**, 198-205 (2020).
32. L. Et-taya, T. Ouslimane, and A. J. S. E. Benami, "Numerical analysis of earth-abundant Cu2ZnSn (SxSe1-x) 4 solar cells based on Spectroscopic Ellipsometry results by using SCAPS-1D," **201**, 827-835 (2020).
33. B. K. Mondal, S. K. Mostaque, M. A. Rashid, A. Kuddus, H. Shirai, J. J. S. Hossain, and Microstructures, "Effect of CdS and In3Se4 BSF Layers on the photovoltaic performance of PEDOT: PSS/n-Si Solar Cells: Simulation based on experimental data," 106853 (2021).
34. M. K. S. B. Rafiq, N. Amin, H. F. Alharbi, M. Luqman, A. Ayob, Y. S. Alharthi, N. H. Alharthi, B. Bais, and M. J. S. r. Akhtaruzzaman, "WS 2: a new window layer material for solar cell application," **10**, 1-11 (2020).
35. A. F. F. Violas, "Novel Rear Contact Architectures in CIGS Solar Cells: Modelling and Experimental Fabrication," 2020).
36. X. Liu, Y. Wang, T. Wu, X. He, X. Meng, J. Barbaud, H. Chen, H. Segawa, X. Yang, and L. J. N. c. Han, "Efficient and stable tin perovskite solar cells enabled by amorphous-polycrystalline structure," **11**, 1-7 (2020).
37. K. Akimoto, S. Ishizuka, M. Yanagita, Y. Nawa, Goutam K. Paul, T. Sakurai, Thin film deposition of Cu2O and application for solar cells,Solar Energy, Volume 80, Issue 6, 2006, Pages 715-722,ISSN 0038-092X, https://doi.org/10.1016/j.solener.2005.10.012.
38. Zeshunji Luo, Licai Fu, Jiajun Zhu, Wulin Yang, Deyi Li, Lingping Zhou, Cu2O as a promising cathode with high specific capacity for thermal battery, Journal of Power Sources,Volume 448,2020,227569,ISSN 0378-7753, https://doi.org/10.1016/j.jpowsour.2019.227569.
39. Tokio Nakada, Microstructural and diffusion properties of CIGS thin film solar cells fabricated using transparent conducting oxide back contacts, Thin Solid Films, Volumes 480–481, 2005, Pages 419-425, ISSN 0040-6090, https://doi.org/10.1016/j.tsf.2004.11.142.
40. Jürgen H. Werner, Julian Mattheis, Uwe Rau, Efficiency limitations of polycrystalline thin film solar cells: case of Cu(In,Ga)Se2,Thin Solid Films, Volumes 480–481, 2005, Pages 399-409, ISSN 0040-6090, https://doi.org/10.1016/j.tsf.2004.11.052.
41. Weimin Li, Wenjie Li, Ye Feng, Chunlei Yang, Numerical analysis of the back interface for high efficiency wide band gap chalcopyrite solar cells, Solar Energy, Volume 180, 2019, Pages 207-215, ISSN 0038-092X, https://doi.org/10.1016/j.solener.2019.01.018.
42. A. Lachgueur and K. Rahmoun, "Simulation and Analysis of Perovskite Solar Cell Based on Germanium," in *ICREEC 2019* (Springer, 2020), pp. 407-412.
43. L. Lin, L. Jiang, P. Li, B. Fan, Y. J. J. o. P. Qiu, and C. o. Solids, "A modeled perovskite solar cell structure with a Cu2O hole-transporting layer enabling over 20% efficiency by low-cost low-temperature processing," **124**, 205-211 (2019).
44. Patel, P.K. Device simulation of highly efficient eco-friendly CH3NH3SnI3 perovskite solar cell. Sci Rep 11, 3082 (2021). https://doi.org/10.1038/s41598-021-82817-w
45. Qu, J., Zhang, L., Wang, H. et al. Simulation of double buffer layer on CIGS solar cell with SCAPS software. Opt Quant Electron 51, 383 (2019). https://doi.org/10.1007/s11082-019-2100-9
46. J. P. Teixeira, R. B. Vieira, B. P. Falcao, M. Edoff, P. M. Salome, and J. P. J. T. J. o. P. C. C. Leitao, "Recombination Channels in Cu (In, Ga) Se2 Thin Films: Impact of the Ga-Profile," **124**, 12295-12304 (2020).

47. L. Zhang, T. Li, Y. Chen, W. Pang, M. Qu, X. Song, Y. Zhang, and H. J. J. o. M. S. M. i. E. Yan, "Influences of donor defect passivation on the performance of Cu (In, Ga) Se 2 thin-film solar cell," **29**, 3482-3491 (2018)
48. P. D. Paulson, R. Birkmire, and W. J. J. o. A. P. Shafarman, "Optical characterization of CuIn 1− x Ga x Se 2 alloy thin films by spectroscopic ellipsometry," **94**, 879-888 (2003).
49. J. D. Dow, "Urbach's Rule," in *Optical Properties of Highly Transparent Solids* (Springer, 1975), pp. 131-143.
50. K. Puech, S. Zott, K. Leo, M. Ruckh, and H. W. J. A. p. l. Schock, "Determination of minority carrier lifetimes in CuInSe2 thin films," **69**, 3375- 77 (1996).
51. C. S. Solanki, *Solar photovoltaics: fundamentals, technologies and applications* (Phi learning pvt. Ltd., 2015).
52. K. J. Z. f. P. Hecht, "Zum Mechanismus des lichtelektrischen Primärstromes in isolierenden Kristallen," **77**, 235-245 (1932).

.